Journal of Autonomous Intelligence (2023) Volume 6 Issue 2
doi: 10.32629/jai.v6i2.938

ORIGINAL RESEARCH ARTICLE

Automated spinal MRI-based diagnostics of disc bulge and desiccating using LS-RBRP with RF

S. Shirly, R. Venkatesan, D. Jasmine David, T. Jemima Jebaseeli*

Computer Science and Engineering, Karunya Institute of Technology and Sciences, Coimbatore 641114, India

*** Corresponding author:** T. Jemima Jebaseeli, jemima_jeba@karunya.edu

ABSTRACT

Low back pain occurs because of the degeneration in Intervertebral Disc (IVD) namely: Disc Desiccation, Disc Bulge, and Disc Herniation, etc. To detect disc degeneration, a doctor often physically evaluates the Magnetic Resonance Imaging (MRI), which takes time and is dependent on the doctor's expertise and training. Degeneration diagnosis that is automated can ease some of the doctor's workload. On 378 IVDs for 63 patients, the proposed method is trained, tested, and assessed. According to the performance evaluation, the proposed Local Sub-Rhombus Binary Relationship (LS-RBRP) and Random Forrest (RF) classifier approach gives an overall accuracy of 90.2%. The proposed approach also produces a higher sensitivity, specificity, precision, and F-score of 80.8%, 90.3%, 90.4%, and 84.5%, respectively, when diagnosing the normal IVD, disc desiccation, and disc bulge in the lumbar MRI.

Keywords: disc desiccation; disc bulge; intervertebral disc; magnetic resonance imaging; random forest

ARTICLE INFO

Received: 7 July 2023
Accepted: 21 July 2023
Available online: 9 August 2023

1. Introduction

As the findings of the World's Burden of Diseases Study, 2010, back pain ranks as one of the most prevalent 10 illnesses that affect 80% of individuals at certain points in their life[1,2]. Low back discomfort is frequently brought on by disc degeneration, including disc desiccation, disc bulge, and disc herniation, among other disc injuries to the lumbar spine[3]. The IVD, which is located among the spinal vertebrae, encompasses two distinct layers, including the center of the nucleus pulposus and the annular fibrosis. Collagen fibers abound in the annulus fibrosis. This structure works as a shock absorber and is well-hydrated. However, due to several circumstances, including trauma, mechanical loading, aging, and genetics, it may degenerate, lose its ability to stay hydrated and become rigid[4].

MRI remains one of the frequently popular approaches for assessing the degeneration of discs because it provides a clear image of the surrounding soft tissues and is harmless[5]. The mid-coronal slice is used for automated categorization of injury to the IVD because it offers an unobstructed view[6]. In the sagittal perspective of the typical disc, the center of the nucleus pulposus appears as bright ellipses, whereas the annulus fibrosis appears as a dark circle encircling the nucleus pulposus. The disc desiccation process causes the IVD to dry out and darken[7].

2. Related works

Several studies on the diagnosis of IVD degeneration have lately been undertaken. Chwialkowski et al.[8] proposed an intensity-based technique for analyzing disc anomalies. Tsai et al.[9] proposed utilizing a boundary approximation approach to locate the ruptured disc. A B-spline curve marks the normal disc border, and the ratio of IVD herniation is determined by extracting convex and concave properties[10]. Then, to categorize normal and herniated discs, k-Nearest Neighbor (k-NN), Nave Bayes, and Support Vector Machine (SVM) are utilized. SVM was used to categorize the IVD after the characteristics were extracted by Beulah and Sharmila[11]. Michopoulou et al.[12] proposed a texture-based approach to detect cervical IVD deterioration. Normal and degenerative discs are then categorized using the LSMD classifier. Hao et al.[13] created an active learning approach to segment the IVD. The normal and degraded IVDs were then distinguished using an SVM classifier. The literature that was previously mentioned tended to merely diagnose herniated IVD and generally deteriorated IVD rather than differentiating between a disc bulge and disc desiccation[14–16]. SVM classifiers were typically employed in the literature to categorize IVD. Because the RF classifier has shown good results in image classification[14].

3. Methodologies

On a sagittal lumbar MRI, **Figure 1** displays the indicated system for diagnosing disc bulging, disc desiccation, and normal. The lumbar IVDs are first segmented using the unsupervised edge segmentation approach, which relies on previous research. Then, using the cutting-edge feature extraction method known as LS-RBRP, the features are extracted from the segmented IVD. To classify the IVD as normal, disc desiccation, or disc bulging, the features are then trained and evaluated using the RF classifier.

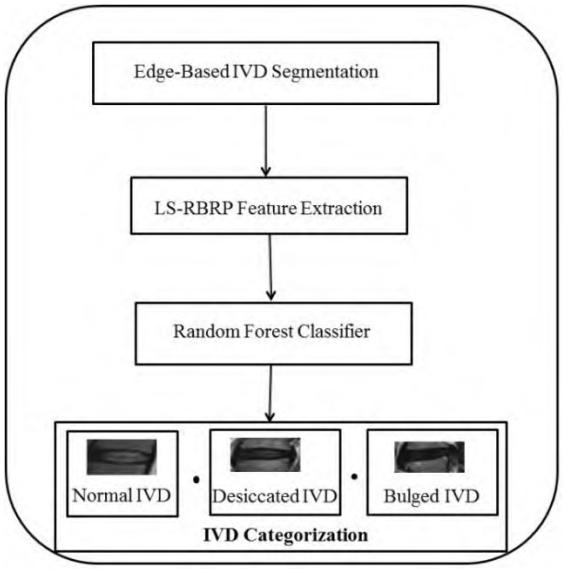

Figure 1. Flow chart for lumbar IVD feature extraction and classification.

3.1. Feature extraction

For feature extraction in this work, the unique spatial domain statistical approach LS-RBRP is applied. LS-RBRP obtains characteristics from every pixel in the ROI, which helps the classifier categorize illnesses and differentiate between normal and abnormal IVDs. The performance of the unique strategy is assessed by comparing it to the methods for extracting features using LBP, LDP, and HOG.

3.1.1. Local sub-rhombus binary relation pattern (LS-RBRP)

An image's rhombus-shaped characteristics are extracted from it using the texture-based feature extraction method known as LS-RBRP. Each pixel in picture I, which has a dimension of $m \times n$ (5 × 5

matrix), has a rhombus built into it. First, the Centre pixel's horizontal ($p^{m,n}$) and perpendicular neighbors are extracted. The neighbours are shown in the image as $p_d^{m,n}$, where d stands for the pixel location of the neighbours closest to the centre pixel. After identifying the pixels perpendicular and horizontal to the center pixels, the final pixels are considered. After extracting every feasible sub-rhombus using the rhombus's center pixels, another sub-rhombus is formed by joining the center pixels of the sub-rhombuses (R_x, x = 1, 2, 3, 4) (R_y). To determine the 4-bit binary vectors of each sub-rhombus, apply Equation (1), and shown in **Figure 2**.

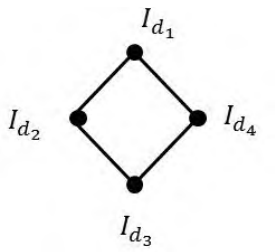

Figure 2. Sub-rhombus numbered in an anti-clockwise direction.

The degree of intensity of the sub-rhombus is shown by $I_{d_1}, I_{d_2}, I_{d_3}, I_{d_4}$. Then, *AND* operation is applied to the remaining sub-rhombuses R_x and R_y.

$$R_x^{'} = R_x \; AND \; R_y \tag{1}$$

At last, using Equation (3), LS-RBRP is calculated to provide a feature vector histogram (31 bin size).

$$LS - RBRP = abs\big((D_1 + D_3) - (D_2 + D_4)\big) \tag{2}$$

In **Figure 3**, part (a) displays the 5 × 5 matrix's neighboring pixel positions, part (b) displays their intensities, part (c) displays the neighboring pixels' intensity values as rhombuses, part (d) displays the rhombus marked in the neighboring pixels' intensities, part (e) shows the sub-rhombus (R_x) pointed out in the adjoining pixels, and part (f) shows the sub-rhombus (R_y) of nearby pixels. **Figure 4** depicts the LS-RBRP calculation. In the proposed approach, the segmented IVD is passed into the LS-RBRP feature extraction algorithm for obtaining the lumbar IVD's properties.

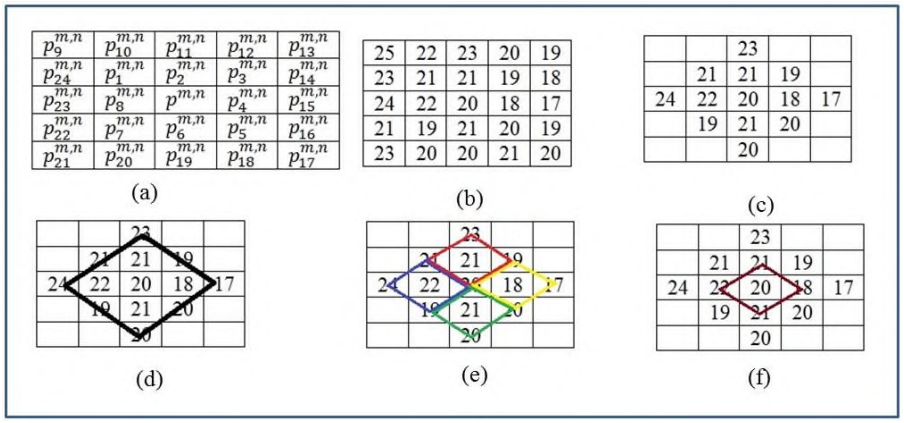

Figure 3. Extraction of the LS-Rhombus neighborhood, **a)** Pixel locations of adjacent pixels; **b)** The intensities of surrounding pixels; **c)** Intensities of adjacent pixels in a rhombus; **d)** Rhombus defined by the brightness of surrounding pixels; **e)** Sub-Rhombuses (R_x) reflected in the brightness of adjoining pixels; **f)** Sub-rhombus (R_y) shown by the brightness of surrounding pixels.

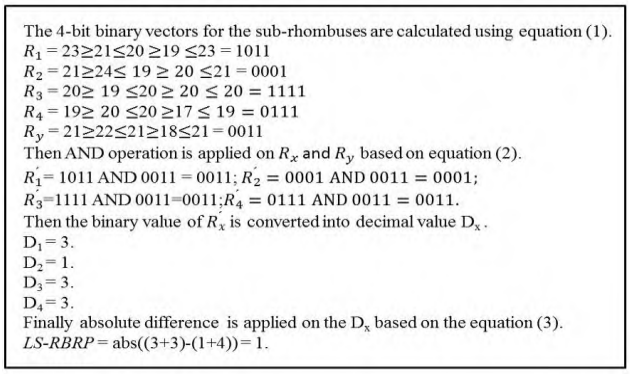

Figure 4. LS-RBRP feature extraction method.

3.1.2. Local binary pattern (LBP)

By segmenting the picture into numerous small parts and extracting its features to create a histogram of 256 bin size feature vector, LBP illustrates the shape and texture of an image. Binary patterns that show the pixels around the regions are among the features. The obtained features are merged into one single histogram. The images are compared by the similarities. It is characterized as a binary comparison of the pixel intensity of the central region and the adjacent pixels.

$$LBP(x_n, y_n) = \sum_{s=0}^{7} K(l_s - l_n)2^s \tag{3}$$

where (x_n, y_n) represents the input pixel location, l_n represents the grey value for the central pixel, l_s represents the grey values of the neighboring pixels, and s represents the number of adjacent pixels.

3.1.3. Local derivative pattern (LDP)

LDP encodes more sophisticated discriminatory characteristics that images cannot provide. It is sometimes referred to as the directed second-order derivative. For the image I with Z general pixel, $I(Z)$ denotes the intensity value of the pixels. $I_{\alpha}^{'}(Z)$ is a first-order derivative with 0°, 45°, 90°, and 135° directions, where $\alpha = 0°, 45°, 90°, 135°$. Z_0 is denoted as a center pixel in the image I, and Z_i denotes the neighboring pixel around the center pixel, where I = 1, …, 8.

3.1.4. Histogram of oriented gradients (HOG)

The intensity variations in the image represent the object's shape and look. The image I begin by dividing them into chunks of cells that form a block. Each cell's HOG is built in an overlapping block. The histogram is then standardized to reduce the regional contrast in each cell block.

3.2. Classification

RF is an ensemble model since it analyses the responses of multiple models for an improved result. Decision trees are a prediction model which derives the goal value from a collection of binary rules. The IVD degeneration is classified using an RF classifier; the extracted LS-RBRP features are trained and evaluated in the random forest approach. The characteristics that are not utilized for training are used for classifier assessment and categorize IVDs as usual, disc drying out, and disc bulging. For assessment, the RF classifier's efficiency corresponds to that of the SVM RBF Kernel classifier.

4. Experimental results

The T2-weighted lumbar MRI for 63 individuals was collected from Rio Scan Centers in Tirunelveli, India. The dimension of the MRI is 448 pixels. The IVDs of each lumbar MRI were classified by the clinician as normal, disc desiccation, and disc bulging. For training, 60% of IVDs are used. The remaining

40% of lumbar IVDs with normal, dehydrated, and inflated IVDs are examined. The classifier is evaluated using its reliability, sensitivity, specificity, accuracy, and F-score performance requirements.

$$Accuracy = \frac{TP + TN}{Total\ number\ of\ samples} \times 100\% \quad (4)$$

$$Sensitivity = \frac{TP}{TP + FN} \times 100\% \quad (5)$$

$$Specificity = \frac{TN}{TN + FP} \times 100\% \quad (6)$$

$$PPV = \frac{TP}{TP + FP} \times 100\% \quad (7)$$

$$F - score = \frac{2TP}{2TP + FP + FN} \times 100\% \quad (8)$$

5. Discussions

Different feature extraction methods (LBP, LDP, and HOG) along with the SVM classifier are compared. The RF classifier outperforms the SVM classifier with all features in terms of all performance indices. The diagnostic result of normal IVDs with different classifiers is shown in **Table 1**.

Table 1. Diagnostic result of normal IVDs with different classifiers.

Metrics	**LBP**		**LDP**		**LS-RBRP**		**HOG**	
	RF	**SVM**	**RF**	**SVM**	**RF**	**SVM**	**RF**	**SVM**
Accuracy (%)	94.7	72.8	92.7	77.4	97.3	78.8	96	88
Sensitivity (%)	42.8	57	57	85.7	71.4	78.5	64	85
Specificity (%)	100	74.4	96.3	76.6	100	78.8	99	89
Precision (%)	100	18.6	61.5	27.2	100	27.5	90	44
F-score (%)	60	28	59.2	41.3	83.3	40.7	75	58

Table 2 gives the diagnostic result of disc bulgesith different classifiers. The performance research also shows that disc bulging and disc desiccation is behind normal cases in terms of classification accuracy.

Table 2. Diagnostic result of disc bulge with different classifiers.

Metrics	**LBP**		**LDP**		**LS-RBRP**		**HOG**	
	RF	**SVM**	**RF**	**SVM**	**RF**	**SVM**	**RF**	**SVM**
Accuracy (%)	87.8	73.5	87.8	69.5	88	70.8	82.7	84
Sensitivity (%)	75.8	43	74	46	77.5	63.5	79	67
Specificity (%)	96.7	92.4	96.7	76.3	94.6	75.2	84	94
Precision (%)	93.6	78	93.4	64.2	90	61.6	76	88
F-score (%)	83.8	55.5	82.6	54	83.3	62.7	77	76

Regarding all three extracted features, the LS-RBRP for RF and SVM provides the highest accuracy; yet, the RF obtains a higher accuracy of 97.3%, which is 18.5% higher in comparison to that of the SVM classification algorithm (78.8%). In terms of performance indices for RF and SVM classifiers based on LBP, LDP, HOG, and LS-RBRP features in disc bulge diagnostics. In this instance, the RF classifier's accuracy is superior to the SVM's for all features. The other RF indices outperform the SVM classifier as well. In the classification of disc bulges, the accuracy of the RF using LS-RBRP parameters is 88%, and this is 14.5% more accurate than the SVM classifier. The SVM using LBP features has a higher accuracy of 73.5%. **Figure 5** shows the result analysis of normal IVDs.

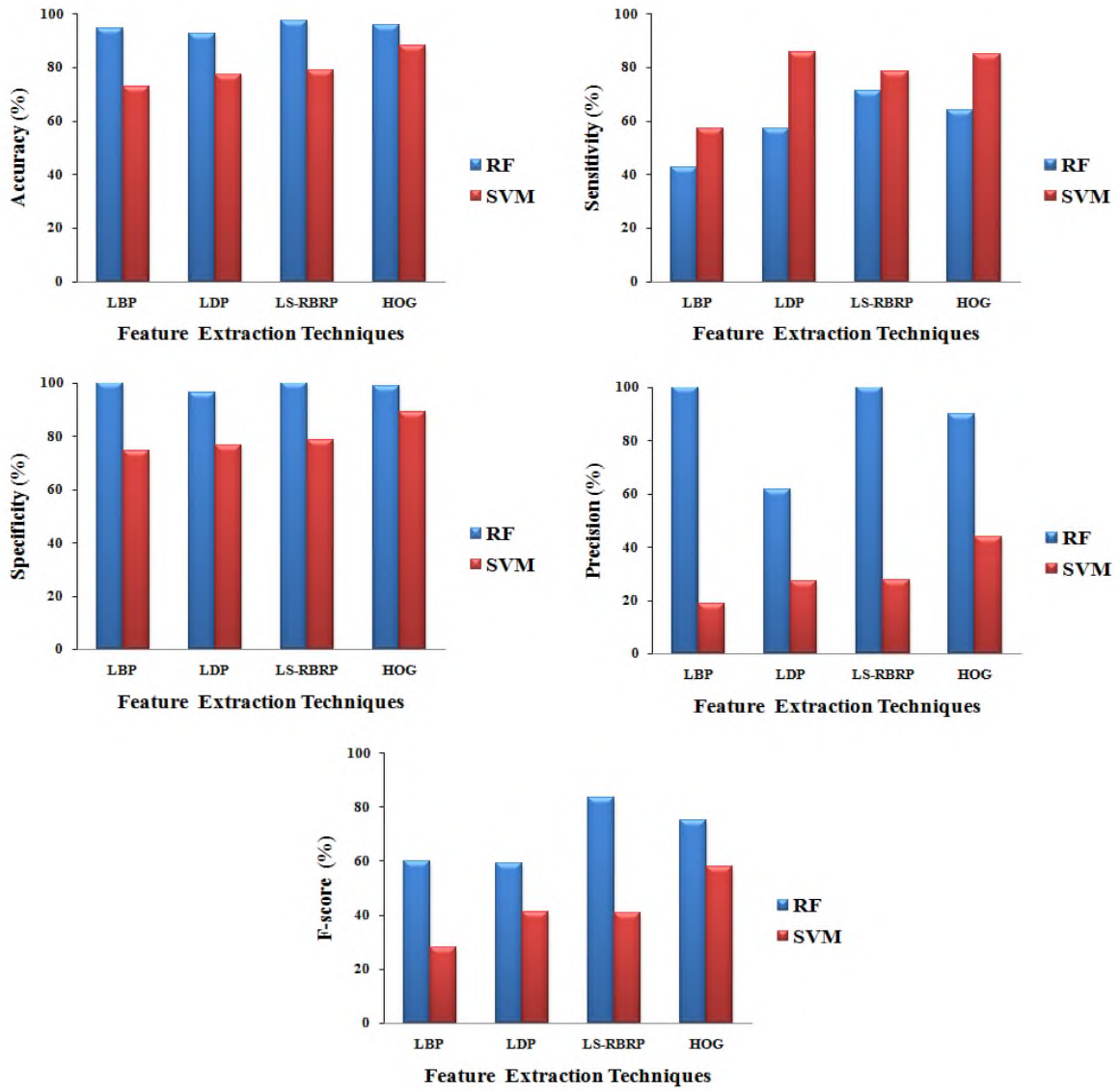

Figure 5. Result analysis of normal IVDs.

According to the performance evaluation, the proposed unique LS-RBRP feature retrieval approach using RF and SVM classifier outperforms the conventional approaches of LBP, LDP, and HOG feature extraction techniques with RF and SVM classifier (**Table 3**).

Table 3. Diagnostic result of disc desiccation with different classifiers.

Metrics	**LBP**		**LDP**		**LS-RBRP**		**HOG**	
	RF	**SVM**	**RF**	**SVM**	**RF**	**SVM**	**RF**	**SVM**
Accuracy (%)	83.4	66.2	84	68	85	66.8	82.7	87
Sensitivity (%)	96.2	65.8	94.9	64.3	93.6	50.6	84	88
Specificity (%)	69.4	66.6	76.3	76.3	76.3	84.7	80	86
Precision (%)	77.5	68.4	81.5	73.8	81.3	78.4	82	87
F-score (%)	85.8	67	87.7	66.6	87	61.5	83	88

Additionally, the RF classifier categorizes the IVDs better than the SVM classifier. In this, the RF recognizes 10 cases as normal and 4 cases as disc desiccation out of 14 independent test cases of normal IVD. SVM, in contrast, properly identifies 11 examples while incorrectly classifying three. Out of 58 disc bulge test instances, 45 are correctly identified in RF and 37 in SVM. The SVM classifier incorrectly

classified 17 cases as normal, while the RF classifier incorrectly classified 74 out of a possible 79 disc desiccation cases as a disc bulge. The total confusion matrix shows that more classes are incorrectly classified by the SVM classifier than by the RF. Additionally, it should be highlighted that the degenerated case is not classified as normal by the RF classifier, which is crucial for automatic diagnosis. **Figure 6** shows the result analysis of disc bulge determined by LBP, LDP, HOG, and LS-RBRP components for RF and SVM classifiers.

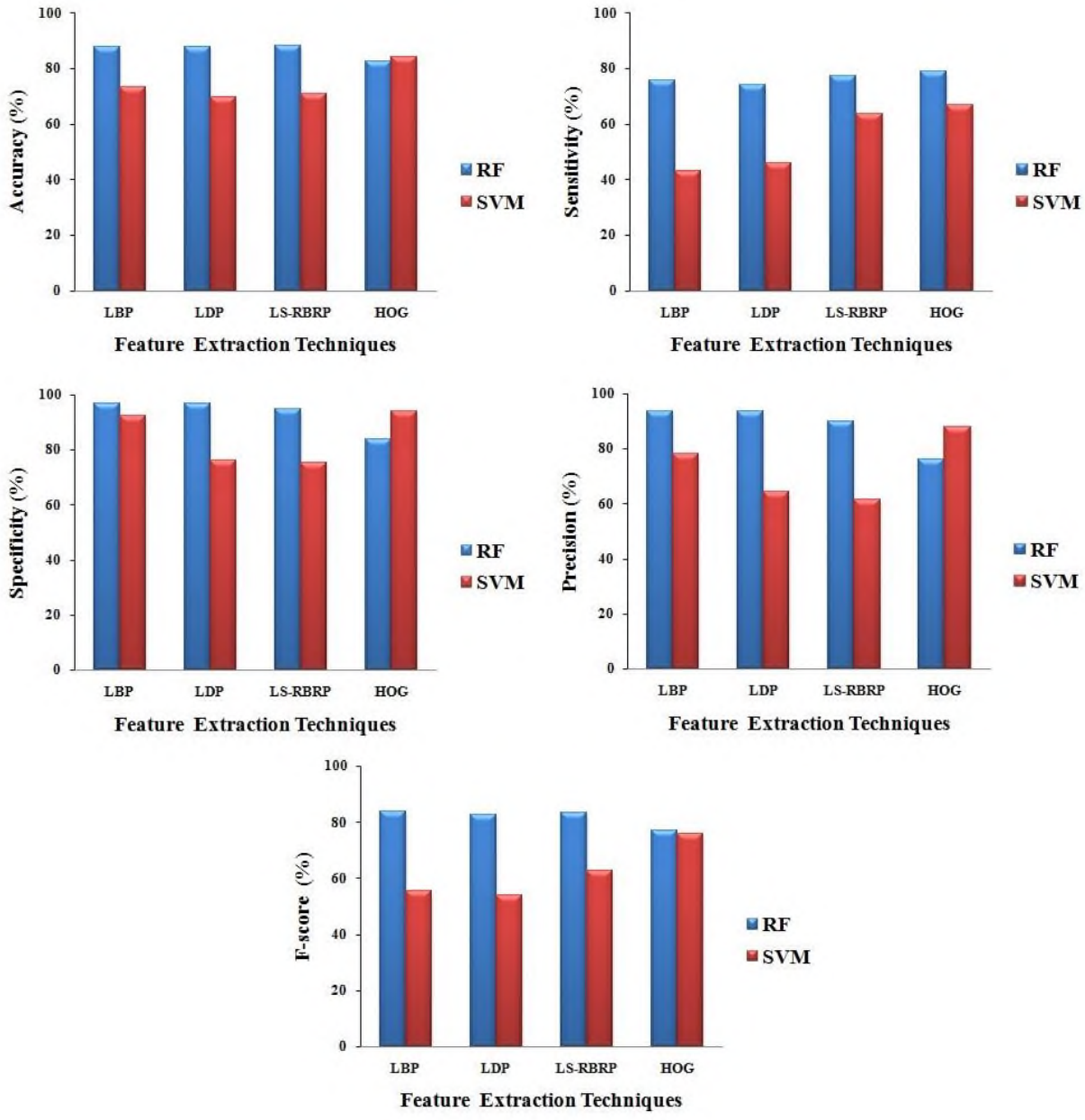

Figure 6. Result analysis of disc bulge.

Figure 7 shows the testing results of disc desiccation as a result of their accuracy indicators determined by LBP, LDP, HOG, and LS-RBRP components for RF and SVM classifiers. In this instance, the RF classifier's accuracy is superior to the SVM's for all features.

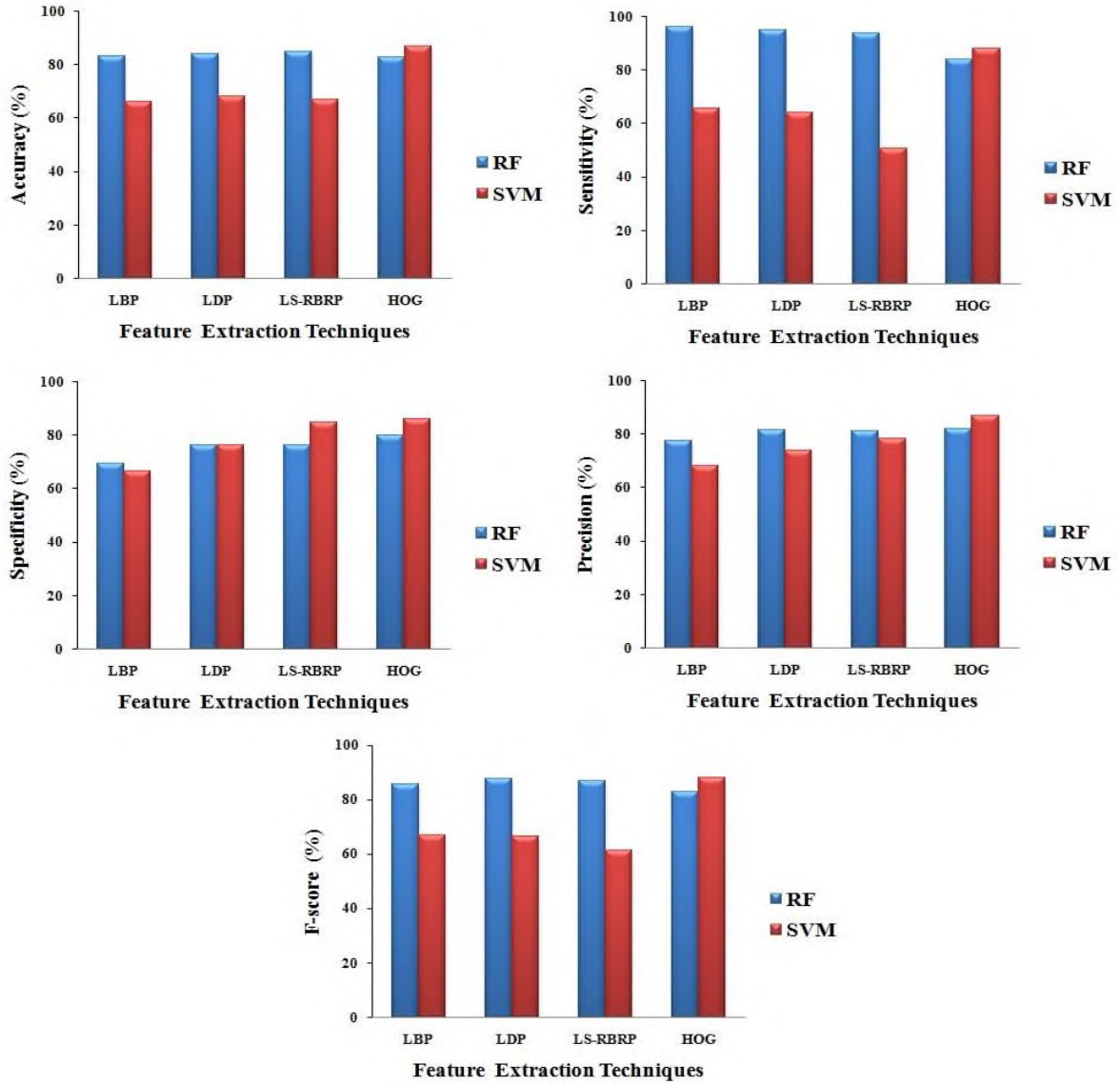

Figure 7. Result analysis of disc desiccation.

6. Conclusions

The proposed study offers an immediate IVD diagnosis. The features are initially extracted using the unique feature extraction method known as LS-RBRP. The lumbar IVD MRI is then categorized using an RF classifier. The proposed system is compared with other feature extraction methods and classifiers to assess the effectiveness of feature extraction and classification. The acquired diagnostic results clearly show that the RF classifier with LS-RBRP gives 90.2% higher accuracy than any other system model in identifying and classifying status from lumbar MRI. In the future, the proposed approach can be used in conjunction with the lumbar MRI disc herniation diagnostic.

Author contributions

Conceptualization, SS; methodology, RV; software, TJJ; validation, DJD; formal analysis, SS; investigation, DJD; resources, SS; data curation, SS; writing—original draft preparation, RV; writing—review & editing, SS; visualization, SS; supervision, SS; project administration, TJJ; funding acquisition, SS and TJJ.

Conflict of interest

The authors declare no conflict of interest.

References

1. Vos T, Flaxman AD, Naghavi M, et al. Years lived with disability (YLDs) for 1160 sequelae of 289 diseases and injuries 1990–2010: A systematic analysis for the Global Burden of Disease Study 2010. *Lancet* 2012; 380(9859): 2163–2196. doi: 10.1016/S0140-6736(12)61729-2
2. Friedly J, Standaert C, Chan L. Epidemiology of spine care: The back pain dilemma. *Physical Medicine and Rehabilitation Clinics of North America* 2010; 21(4): 659–677. doi: 10.1016/j.pmr.2010.08.002
3. Oktay AB, Albayrak NB, Akgul YS. Computer aided diagnosis of degenerative intervertebral disc diseases from lumbar MR images. *Computerized Medical Imaging and Graphics* 2014; 38(7): 613–619. doi: 10.1016/j.compmedimag.2014.04.006
4. Modic MT, Ross JS. Lumbar degenerative disk disease. *Radiology* 2007; 245(1): 43–61. doi: 10.1148/radiol.2451051706
5. Remonda L, Lukes A, Schroth G. Spinal stenosis: Current aspects of imaging diagnosis and therapy. *Schweizerische Medizinische Wochenschrift* 1996; 126(6): 220–229.
6. Castro-Mateos I, Pozo JM, Lazary A, Frangi AF. 2D segmentation of intervertebral discs and its degree of degeneration from T2-weighted magnetic resonance images. In: Aylward S, Hadjiiski LM (editors). *Medical Imaging 2014: Computer-Aided Diagnosis.* SPIE; 2014.
7. Michopoulou SK, Costaridou L, Panagiotopoulos E, et al. Atlas-based segmentation of degenerated lumbar intervertebral discs from MR images of the spine. *IEEE Transactions on Biomedical Engineering* 2009; 56(9): 2225–2231. doi: 10.1109/TBME.2009.2019765
8. Chwialkowski MP, Shile PE, Peshock RM, et al. Automated detection and evaluation of lumbar discs in MR images. In: Images of the Twenty-First Century. Proceedings of the Annual International Engineering in Medicine and Biology Society; 9–12 November 1989; Seattle, WA, USA. pp. 571–572.
9. Tsai MD, Jou SB, Hsieh MS. A new method for lumbar herniated inter-vertebral disc diagnosis based on image analysis of transverse sections. *Computerized Medical Imaging and Graphics* 2002; 26(6): 369–380. doi: 10.1016/S0895-6111(02)00033-2
10. Ghosh S, Raja'S A, Chaudhary V, Dhillon G. Composite features for automatic diagnosis of intervertebral disc herniation from lumbar MRI. *2011 Annual International Conference of the IEEE Engineering in Medicine and Biology Society* 2011; 2011: 5068–5071. doi: 10.1109/IEMBS.2011.6091255
11. Beulah A, Sharmila TS. Classification of intervertebral disc on lumbar MR images using SVM. In: Proceedings of 2016 2nd International Conference on Applied and Theoretical Computing and Communication Technology (iCATccT); 21–23 July 2016; Bangalore, India. pp. 293–297.
12. Michopoulou S, Boniatis I, Costaridou L, et al. Computer assisted characterization of cervical intervertebral disc degeneration in MRI. *Journal of Instrumentation* 2009; 4(5): P05022. doi: 10.1088/1748-0221/4/05/P05022
13. Hao S, Jiang J, Guo Y, Li H. Active learning based intervertebral disk classification combining shape and texture similarities. *Neurocomputing* 2013; 101: 252–257. doi: 10.1016/j.neucom.2012.08.008
14. Sunassee S, Mungur A, Armoogum S, Pudaruth S. A comprehensive review on congestion control techniques in networking. In: Proceedings of 2021 5th International Conference on Computing Methodologies and Communication (ICCMC); 8–10 April 2021; Erode, India. pp. 305–312.
15. Devi RM, Premkumar M, Jangir P, et al. IRKO: An improved Runge-Kutta optimization algorithm for global optimization problems. *Computers, Materials & Continua* 2022; 70(3): 4803–4827. doi: 10.32604/cmc.2022.020847
16. Ramasamy MD, Periasamy K, Krishnasamy L, et al. Multi-disease classification model using strassen's half of threshold (SHoT) training algorithm in healthcare sector. *IEEE Access* 2021; 9: 112624–112636. doi: 10.1109/ACCESS.2021.3103746